

****FULL TITLE****

ASP Conference Series, Vol. ****VOLUME****, © ****YEAR OF PUBLICATION****

****NAMES OF EDITORS****

Mid-Infrared Spectral Indicators of Star-Formation and AGN Activity in Normal Galaxies

Marie Treyer

California Institute of Technology, MC 278-17, 1200 E. California Boulevard, Pasadena, CA 91125, USA

Ben Johnson

Institute of Astronomy, University of Cambridge, Madingley Road, Cambridge CB3 0HA, UK

David Schiminovich and Matt O’Dowd

Astronomy Department, Columbia University, 550 W. 120 St., New York, NY 10027, USA

Abstract. We investigate the use of mid-infrared PAH bands, continuum and emission lines as probes of star-formation and AGN activity in a sample of 100 ‘normal’ and local ($z \sim 0.1$) galaxies. The MIR spectra were obtained with the *Spitzer* IRS as part of the Spitzer-SDSS-GALEX Spectroscopic Survey (SSGSS) which includes multi-wavelength photometry from the UV to the FIR and optical spectroscopy. The spectra were decomposed using PAHFIT (Smith et al. 2007), which we find to yield PAH equivalent widths (EW) up to ~ 30 times larger than the commonly used spline methods. Based on correlations between PAH, continuum and emission line properties and optically derived physical properties (gas phase metallicity, radiation field hardness), we revisit the diagnostic diagram relating PAH EWs and $[\text{Ne II}]12.8\mu\text{m}/[\text{O IV}]25.9\mu\text{m}$ and find it more efficient as distinguishing weak AGNs from star-forming galaxies than when spline decompositions are used. The luminosity of individual MIR component (PAH, continuum, Ne and H_2 lines) are found to be tightly correlated to the total IR luminosity and can be used to estimate dust attenuation in the UV and in $\text{H}\alpha$ lines based on energy balance arguments.

1 Goals

We aim at determining the main source of ionizing radiation and star-formation rate of normal galaxies from MIR spectroscopy.

2 The SSGSS Sample

The Spitzer-SDSS-GALEX Spectroscopic Survey is an IRS survey of 100 local galaxies in the Lockman Hole. The data include GALEX FUV photometry, SDSS optical imaging and spectroscopy, Spitzer IRAC and MIPS photometry. The sample has a surface brightness limit of 0.75 MJy sr^{-1} at $5.8\mu\text{m}$ and a flux limit of 1.5 mJy at $24\mu\text{m}$. It was selected to cover the range of physical properties

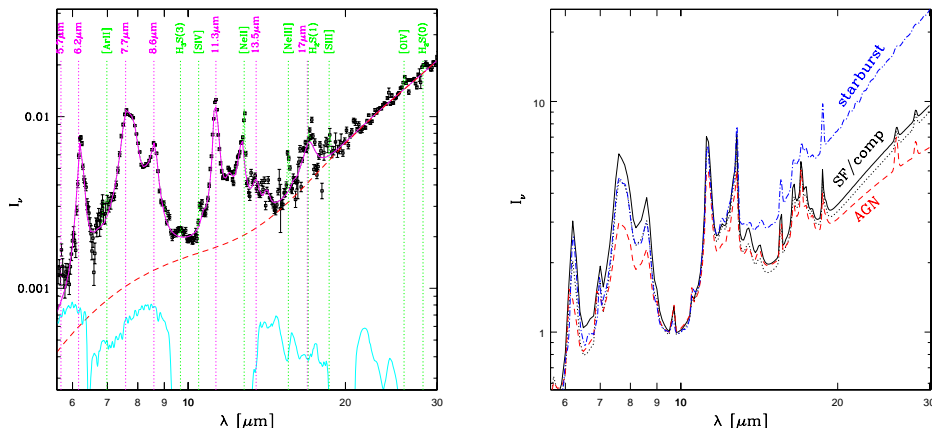


Figure 1. *Left:* Example spectrum (a SF galaxy) with PAHFIT decomposition: continuum (dashed red line), PAH features (solid purple line) and emission lines (dotted green line). The lower curves show - from left to right - the filter responses of the IRAC bands at 6 and 8 μm , of the IRS blue Peak Up band at 16 μm and of the MIPS band at 24 μm bands. *Right:* The mean spectra of SF galaxies (solid line), composite galaxies (dotted line) and AGNs (dashed line). The dot-dashed line is the average starburst spectrum of Brandl et al. (2006). The spectra are normalized at 10 μm .

of ‘normal’ galaxies (e.g. $9.3 \leq \log(M/M_\odot) \leq 11.3$, $8.7 \leq \log(\text{O}/\text{H}) + 12 \leq 9.2$, $0.4 < A_{\text{H}\alpha} < 2.3$). The redshifts span $0.03 < z < 0.21$ with a mean of 0.1 similar to that of the full SDSS spectroscopic sample. Galaxies are classified as star-forming (black dots), composite (pink stars) or AGN (red triangles) according to the boundaries of Kewley et al. (2001) and Kauffmann et al. (2003) on the $[\text{N II}]\lambda 6583/\text{H}\alpha$ versus $\phi 3\text{hb}$ ‘‘BPT’’ diagram (Baldwin et al. 1981). First results were reported by O’Dowd et al. (2009).

3 Spectral Decomposition

We used PAHFIT (Smith et al. 2007) to decompose the spectra into a sum of dust attenuated thermal dust continuum, PAH features and emission lines. The left panel of Fig. 1 shows an example decomposition for a typical SF galaxy. The right panel shows the mean spectra of SF galaxies, composite galaxies and AGNs along with the average starburst spectrum of Brandl et al. (2006). The transition from starburst to SF galaxy to AGN is marked by a declining continuum slope, decreased $[\text{Ne II}]\lambda 12.8\mu\text{m}$ and $[\text{S III}]\lambda 18.7\mu\text{m}$ emission and enhanced $[\text{O IV}]\lambda 25.9\mu\text{m}$ emission. The AGN spectrum, and to a lesser extent the starburst spectrum, show weaker PAH emission at low wavelength than the SF spectrum, an effect attributed to the destruction of PAHs in intense far-UV radiation fields.

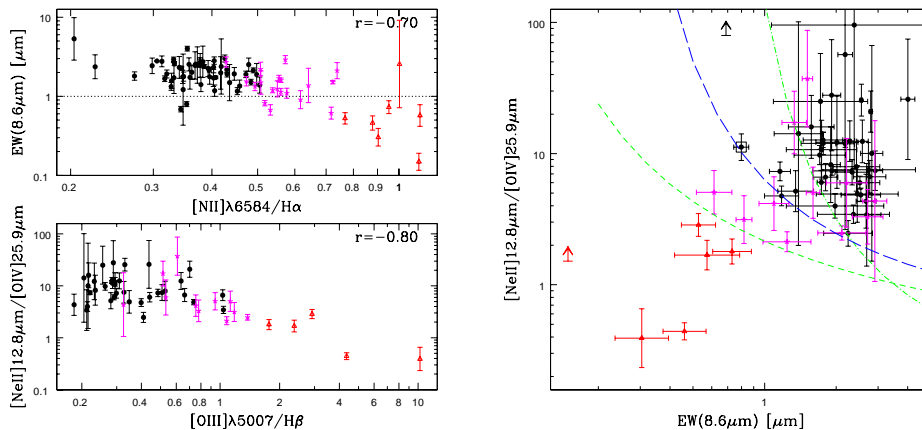


Figure 2. *Top Left:* 8.6 μm PAH EW versus [N II]λ6583/Hα. The dotted line is an empirical lower limit for SF galaxies ($EW(8.6\mu\text{m}) > 1\mu\text{m}$). *Bottom left:* [Ne II]12.8 μm/[O IV]25.9 μm versus $\phi 3\text{hb}$. SF galaxies are represented as black dots, composite galaxies as pink stars and AGNs as open red triangles. r is the Pearson correlation coefficient. *Right:* 8.6 μm PAH EWs against [Ne II]12.8 μm/[O IV]25.9 μm. This version of the Genzel et al. (1998) diagram resembles a flipped version of the optical Baldwin et al. (1981) diagram. The short-dashed lower line and the dot-dashed upper line are the Kewley et al. (2001) and Kauffmann et al. (2003) optical boundaries translated into the MIR plane using the correlations in the left panels. The long-dashed middle line is an empirical boundary marking the region below which we do not find any optically defined SF galaxy.

4 Conclusions

- We find systematic trends between MIR spectral properties and optically derived physical properties, in particular between short wavelength PAH EWs and [N II]λ6583/Hα (gas phase metallicity), and between [Ne II]12.8 μm/[O IV]25.9 μm versus $\phi 3\text{hb}$ (radiation field hardness) (Fig. 2, left panel);
- The Genzel et al. (1998) diagram has better resolution using PAHFIT than spline decompositions. It is very similar to the optical “BPT” diagram (Fig. 2, right panel). The mixed SF/composite region may be revealing obscured AGNs in a large fraction of optically defined “pure” SF galaxies.
- The PAH, continuum, Ne and H₂ luminosities are tightly and nearly linearly correlated to the total IR luminosity, less so to the dust corrected Hα luminosity (SFR) (Fig. 3, left panel);
- Following Kennicutt et al. (2009), the MIR components can be used to estimate dust attenuation in Hα and UV based on energy balance arguments (Fig. 3, right panel).

References

- Baldwin, J. A., Phillips, M. M., & Terlevich, R. 1981, PASP, 93, 5
 Brandl, B. R., Bernard-Salas, J., Spoon, H. W. W., Devost, D., Sloan, G. C., Guilles, S., Wu, Y., Houck, J. R., Weedman, D. W., Armus, L., Appleton, P. N., Soifer,

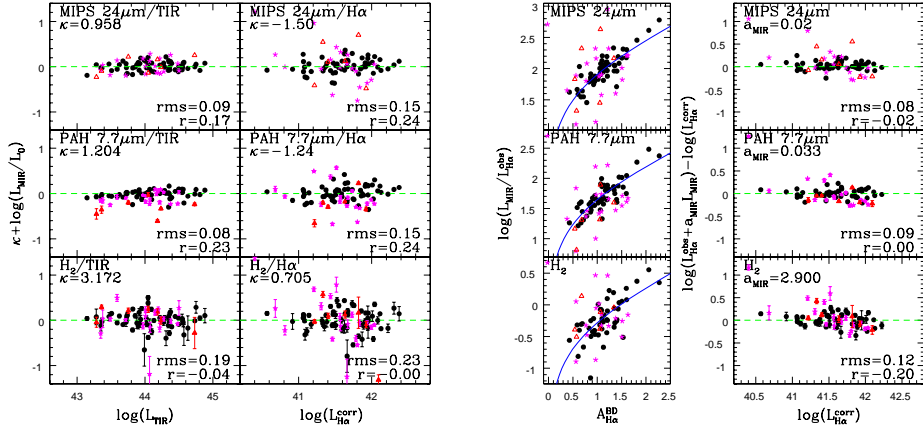


Figure 3. *Column 1:* L_{MIR}/L_{TIR} ratios as a function of L_{TIR} where L_{MIR} equals - from top to bottom - the $24\mu\text{m}$ MIPS band luminosity (νL_ν), the luminosity of the $7.7\mu\text{m}$ PAH complex and the H_2 luminosity where H_2 is defined as the sum of the $S(0)$ to $S(2)$ rotational lines. The logarithmic scaling factors κ are defined as the mean of $\log(L_{TIR}/L_{MIR})$ for the SF population alone (green dashed lines). The rms and Pearson coefficient r are also for the SF population alone. *Column 2:* $L_{MIR}/L_{H\alpha}^{corr}$ ratios as a function of $L_{H\alpha}^{corr}$ (the dust corrected $\text{H}\alpha$ luminosity). *Column 3:* $L_{MIR}/L_{H\alpha}^{obs}$ ratios (observed $\text{H}\alpha$ luminosity) against $\text{H}\alpha$ attenuation measured from the Balmer decrement. The solid lines are best fits to $A_{H\alpha} = 2.5 \log [1 + a_{MIR} L_{MIR}/L_{H\alpha}^{obs}]$ (Kennicutt et al. 2009). *Column 4:* $L_{H\alpha}^{obs} + a_{MIR} L_{MIR}$ to $L_{H\alpha}^{corr}$ ratios as a function of $L_{H\alpha}^{corr}$. The a_{MIR} coefficients derived in the previous column are indicated at the top left of each panel.

- B. T., Charmandaris, V., Hao, L., Higdon, J. A. M. S. J., & Herter, T. L. 2006, ApJ, 653, 1129
- Genzel, R., Lutz, D., Sturm, E., Egami, E., Kunze, D., Moorwood, A. F. M., Rigopoulou, D., Spoon, H. W. W., Sternberg, A., Tacconi-Garman, L. E., Tacconi, L., & Thatte, N. 1998, ApJ, 498, 579
- Kauffmann, G., Heckman, T. M., Tremonti, C., Brinchmann, J., Charlot, S., White, S. D. M., Ridgway, S. E., Brinkmann, J., Fukugita, M., Hall, P. B., Ivezić, Ž., Richards, G. T., & Schneider, D. P. 2003, MNRAS, 346, 1055
- Kennicutt, R. C., Hao, C., Calzetti, D., Moustakas, J., Dale, D. A., Bendo, G., Engelbracht, C. W., Johnson, B. D., & Lee, J. C. 2009, ApJ, 703, 1672
- Kewley, L. J., Dopita, M. A., Sutherland, R. S., Heisler, C. A., & Trevena, J. 2001, ApJ, 556, 121
- O'Dowd, M. J., Schiminovich, D., Johnson, B. D., Treyer, M. A., Martin, C. D., Wyder, T. K., Charlot, S., Heckman, T. M., Martins, L. P., Seibert, M., & van der Hulst, J. M. 2009, ApJ, 705, 885
- Smith, J. D. T., Draine, B. T., Dale, D. A., Moustakas, J., Kennicutt, Jr., R. C., Helou, G., Armus, L., Roussel, H., Sheth, K., Bendo, G. J., Buckalew, B. A., Calzetti, D., Engelbracht, C. W., Gordon, K. D., Hollenbach, D. J., Li, A., Malhotra, S., Murphy, E. J., & Walter, F. 2007, ApJ, 656, 770